# Spectra of secondary electrons generated in water by energetic ions

Emanuele Scifoni,[1,*] Eugene Surdutovich,[1,2] and Andrey V. Solov'yov[1,†]
[1]*Frankfurt Institute for Advanced Studies, Ruth-Moufang-Str. 1, 60438 Frankfurt am Main, Germany*
[2]*Department of Physics, Oakland University, Rochester, Michigan 48309, USA*
(Received 1 November 2009; published 2 February 2010)

The energy distributions of secondary electrons produced by energetic carbon ions (in the energy range used, e.g., in hadron therapy), incident on liquid water, are discussed. For low-energy ions, a parametrization of the singly differential ionization cross sections is introduced, based on tuning the position of the Bragg peak. The resulting parametrization allows a fast calculation of the energy spectra of secondary electrons at different depths along the ion's trajectory, especially near the Bragg peak. At the same time, this parametrization provides penetration depths for a broad range of initial-ion energies within the therapeutically accepted error. For high-energy ions, the energy distribution is obtained with a use of the dielectric-response function approach. Different models are compared and discussed.

DOI: 10.1103/PhysRevE.81.021903 PACS number(s): 87.53.−j, 61.80.−x, 41.75.Ak, 34.50.Bw

## I. INTRODUCTION

An accurate energy distribution of electrons produced as a result of the ionization of water molecules induced by fast incident ions is a key piece of information for many applications. One of the most important among these applications, since liquid water is considered to be a good tissuelike medium, is related to its relevance to the physics of ion-beam cancer therapy and radiation protection in space. Ion beam cancer therapy has become an operative treatment tool, whose power is based on theoretical and computational methods of basic science [1]. On the other hand, radiation damage by ions is becoming a major topic of research for shielding of human space missions by the ESA and NASA [2]. These two fields of applications differ slightly in the initial energies of incident ions, hundreds of MeV/u for cancer therapy and $\sim$1 GeV/u for radiation protection from galactic cosmic rays.

The goal of studies applied to both curing and shielding purposes is an understanding and controlling of the radiation damage, which is focused on DNA damage and its repair. Many details of the involved physical processes, starting from the incidence of an energetic ion on tissue and leading to biological damage, are still far from being explained and calculated on a nanoscopic level. An attempt to build an inclusive picture of relevant physical processes was suggested in our previous work [3,4], which proposed a multiscale approach to this problem.

It is widely accepted that the major part of damage done by ions is related, directly or indirectly, to the secondary electrons produced by ionization of the medium. These electrons may interact with parts of DNA molecules in the cell nuclei, generate other secondaries, such as other electrons or radicals, which can then interact with DNA. Secondary electrons also participate in energy transfer leading to thermal spikes [5] which contribute to biomolecular damage. Finally each ionization produces a hole which may also cause DNA damage.

In the multiscale approach [3], the energy spectrum of secondary electrons occupies the key position. It is also an important input for numerous Monte Carlo (MC) simulations of track structure [6–8]. An increasing interest for a more accurate shape of this distribution, especially at low energies, has followed the well-known experiments by the Sanche's group [9] revealing possible damage induced by low-energy ($<$10 eV) electrons.

The studies of the energy distribution of secondary electrons have been carried out by different groups (e.g., [8,10]). In a majority of works, energetic electrons or protons are the primary projectiles [10,11]; while a few studies have been extended to heavier ions [12,13]. In our analysis, we consider carbon ions because they have been largely used in ion-beam therapy both in Germany and Japan [14]. However, our analysis can also be extended to other ions.

The difficulties in analyzing singly differential ionization cross sections are basically of two types: (1) the impossibility to depict all energy ranges using the same formalism because the energy range of interest is too large to be included in the range of validity of a single approximation; (2) the deviation of the ion's propagation through liquid water from that of water vapor often used in experiments, is unknown. As the applicability of the Born approximation is a key issue in this connection, we divide our analysis (as it is usual in similar works [8,10]) between the fast and relatively slow regimes of the projectile's velocity, corresponding to different parts of the ion's trajectory. First, we start with a general approach valid for slow ions. This approach is the only possibility in that energy range, and the accuracy in the shape of secondary electron spectra is limited in the entire energy range. Then, we present a method valid only for fast ions, but returning more accurate electron energy distributions in that range.

## II. SLOW REGIME

In order to account for the region where the ion's energy is smaller than 500 keV/u, where the Born approximation is not valid, we use a parametric approach built on existing experimental data. As was shown in our previous papers

*scifoni@fias.uni-frankfurt.de
†solovyov@fias.uni-frankfurt.de

 

TABLE I. Fitting parameters for the two inner shells of the water molecule $(1a_1, 2a_1)$ and for the three outer shells $(1b_2, 3a_1, 1b_1)$ in the original parametrization by Rudd for vapor [18] and in a parametrization here introduced for liquid.

| | Parameter | $A_1$ | $B_1$ | $C_1$ | $D_1$ | $E_1$ | $A_2$ | $B_2$ | $C_2$ | $D_2$ | $\alpha$ |
|---|---|---|---|---|---|---|---|---|---|---|---|
| Inner shell | | 1.25 | 0.5 | 1.0 | 1.0 | 3.0 | 1.1 | 1.3 | 1.0 | 0.0 | 0.66 |
| Outer shell | Vapor[a] | 0.97 | 82 | 0.4 | −0.3 | 0.38 | 1.04 | 17.3 | 0.76 | 0.04 | 0.64 |
| Outer shell | Liquid (this work) | 1.02 | 82 | 0.50 | −0.78 | 0.38 | 1.07 | 14.5 | 0.61 | 0.04 | 0.64 |

[a]Reference [18].

[15,16], the probability to produce $dN$ secondary electrons with kinetic energies from $W$ to $W+dW$, $\frac{dN}{dW}dW$, from a segment of the ion track $d\zeta$, is proportional to $\frac{d\sigma}{dW}d\zeta$, where $\frac{d\sigma}{dW}$ is the singly differential ionization cross section (SDCS). This cross section is the main characteristic in our analysis defining both the ion's stopping in the medium and the energy spectrum of secondary electrons.

Since the angular distribution of prevailing low-energy electrons ($W<45$ eV) is rather flat over the whole angular range [17], the SDCS is sufficient for our analysis. Besides the kinetic energy of secondary electrons and the properties of water molecules, the SDCS depends on the kinetic energy of projectiles, $T$, and their charges, $z$.

### A. Semiempirical model for vapor water

In our previous papers [15,16], we used a model based on a parametrization by Rudd [18], which yields an analytical formula for SDCS on a wide energy range combining the experimental data for water vapor, calculations within the plane-wave Born approximation, and other theoretical models. This model, original for protons, has been extended first to helium [12] and then to heavier ions by us [15,16] and a few other works [19,20].

We used the following parametric functions [16]:

$$\frac{d\sigma(W,T)}{dW} = z_{eff}^2 \sum_i \frac{4\pi a_0^2 N_i}{I_i}\left(\frac{R}{I_i}\right)^2 \times \frac{F_1^i(v_i) + F_2^i(v_i)\omega_i}{(1+\omega_i)^3\{1+\exp[\alpha^i(\omega_i-\omega_i^{\max})/v_i]\}}, \quad (1)$$

$$F_1^i(v) = A_1^i \frac{\ln\left(\frac{1+v^2}{1-\beta^2}\right)-\beta^2}{B_1^i/v^2+v^2} + \frac{C_1^i v^{D_1^i}}{1+E_1^i v^{D_1^i+4}}, \quad (2)$$

$$F_2^i(v) = C_2^i v^{D_2^i} \frac{A_2^i v^2 + B_2^i}{C_2^i v^{D_2^i+4} + A_2^i v^2 + B_2^i}. \quad (3)$$

where the sum is taken over the electron shells of the water molecule, $a_0$ is the Bohr radius, $R$ is the Rydberg, $N_i$ the shell occupancy, $I_i$ the ionization potential of the shell, $\omega_i = W/I_i$, $v_i = (mV^2/(2I_i))^{1/2}$, $\omega_i^{\max} = 4v_i^2 - 2v_i - R/(4I_i)$; $m$ is the mass of electron, $V$ is the velocity of the projectile, $T$ its kinetic energy and $\beta = V/c$.

The corresponding fitting parameters, taken from Ref. [18], $A_1^i \ldots E_1^i$, $A_2^i \ldots D_2^i$, and $\alpha^i$ are listed in Table I and the ionization potentials in Table II (vapor row).

This parametrization is different from the original [18] in two respects: first, the expression for $F_1$ is modified so that it has the correct asymptotic behavior in the relativistic limit [16], and second, it contains an effective charge of the ion $z_{eff}$, which depends on the velocity of the ion. The effective charge takes into account the effect of charge transfer, i.e., gradual reduction in the original charge of the ion as it slows down. For the effective charge, we have used an expression given by Barkas [21], $z_{eff} = z[1-\exp(-125\beta z^{-2/3})]$.

These two modifications give the shape of the LET dependence along the track for a single ion. However, ions in the beam are spread in energies due to scattering. The straggling in energies is taken into account in Ref. [16], but more details are given in Ref. [22]. All in all, our resulting general parametrization of SDCS for water yielded a 97% accuracy in reproducing the Bragg's peak position in comparison with experiment and compared very well with MC simulations [23] in shape (without nuclear fragmentation).

### B. Semiempirical model extensions for liquid water

However, the parametrization for SDCS, used in Refs. [16,22], did not take into account medium density effects, i.e., the effects arising from the difference between the ion's propagation in liquid water from that of vapor. We used the liquid-water density, but took all other parameters corresponding to water vapor. Unfortunately, the experimental data for ionization cross sections in liquid water are very limited and insufficient for making an independent parametrization. However, since the SDCS of ionization along with excitation contribute to the stopping cross section, directly related to LET [16], it is possible to extract a modified parametrization of the SDCS for liquid water from different available experiments. In Ref. [10], the experimental measurements of stopping cross sections [24] are used as a function of the ion's energy. This only provides a single curve to which to compare. Instead, we choose to fit the parametrization with measurements of the LET dependence on the pen-

TABLE II. Ionization potentials for vapor [18] and liquid [35] water (in eV). In the two approaches presented in this paper, the first and the second set are respectively used.

| Shell | $1b_1$ | $3a_1$ | $1b_2$ | $2a_1$ | $1a_1$ |
|---|---|---|---|---|---|
| Vapor | 12.61 | 14.73 | 18.55 | 32.2 | 539.7 |
| Liquid | 10.79 | 13.39 | 16.05 | 32.3 | 539.0 |

TABLE III. Energies and parameters for excitation cross sections (Eq. (5)) corresponding respectively to states $A^1B_1$, $B^1A_1$, Rydberg $A+B$, and Rydberg $C+D$, and diffuse bands.

| $k$ | $E_k$ (eV) | $a_k$ | $b_k$ | $c_k$ |
|---|---|---|---|---|
| 1 | 8.17 | 2245 | 4493 | 0.85 |
| 2 | 10.13 | 6319 | 7020 | 0.88 |
| 3 | 11.31 | 4387 | 8135 | 0.88 |
| 4 | 12.91 | 989 | 3172 | 0.78 |
| 5 | 14.50 | 1214 | 3352 | 0.78 |

etration depth in liquid water. These depths have been measured at GSI [25,26]. This not only provides several curves at different initial energies, but also a direct comparison with the carbon ion data. So instead of tuning parameters directly to the stopping cross sections as in [10], we use the reported Bragg-peak profiles, for different initial-ion energies and thus the LET as a function of the penetration depth.

In fact, the integration of the inverse of the LET gives the position of the Bragg peak. Hence, we can adjust the parameters of the SDCS by tuning the depth of the Bragg peak to the experiment. Such a procedure is rather simple and fast using our approach [16].

So, we start with the SDCS of ionization, which includes relativistic effects and charge transfer as an input to the stopping cross section, defined as

$$\sigma_{\rm st} = \sum_i \int_0^{W_{\rm max}} (W + I_i) \frac{d\sigma_i(W,T)}{dW} dW. \tag{4}$$

Now, we need to add the contribution of excitation to the stopping cross section. These cross sections are accounted by scaling with our effective charge, depending on ions' velocities, a semiempirical formulation by Miller and Green [27] for protons

$$\sigma_{exc,k}(T) = z_{eff}^2 \frac{a_k(T - E_k)}{b_k + T^{c_k}}, \tag{5}$$

where the index $k$ corresponds to five different excitation transitions, i.e., to states $A^1B_1$, $B^1A_1$, Rydberg $A+B$, Rydberg $C+D$, and diffuse bands, respectively; $\sigma_{exc,k}(T)$ is the excitation cross section, $E_{exc,k}$ is the corresponding excitation energy and $a_k, b_k, c_k$ are parameters reported in Table III and computed from data reported and fully explained in Refs. [10,27], giving cross sections in Å$^2$ when energy is input in eV. The stopping cross section is then calculated [16] as

$$\sigma_{\rm st}^*(T) = \sigma_{\rm st}(T) + \sum_i E_{exc,i}\sigma_{exc,i}(T). \tag{6}$$

The LET is given by $n\sigma_{\rm st}^*(T)$, where $n$ is a number density of liquid-water molecules.

At this point, we add the energy straggling correction, i.e., a widening of the peak arising from the stocasticity of the energy-loss phenomenon and related to the multiple scattering of ions. This correction affects also the position of the Bragg peak, slightly reducing its depth. The correction is given by

$$\left\langle \frac{dT}{dx}(x) \right\rangle = \frac{1}{\sigma_{str}(x_0)\sqrt{2\pi}} \int_0^{x_0} \frac{dT}{dx}(x') \exp\left( -\frac{(x'-x)^2}{2\sigma_{str}(x_0)^2} \right) dx', \tag{7}$$

where $x_0$ is a maximum penetration depth of the projectile, and $\sigma_{str}(x_0) = 0.012 x_0^{0.951}/\sqrt{A}$ is the longitudinal-straggling standard deviation (in cm, when $x_0$ is also in cm) computed with a phenomenological formula introduced by Chu [28], and depending (through $x_0$) on the initial energy of the ion $T_0$. $A$ is the ion's mass number. We found, that if we gradually change the parameters from Rudd's model within the experimental error [18], the Bragg-peak position can be tuned to match those obtained in stopping-power experiments (see Fig. 1), as well as MC transport code simulation (MCHIT code based on GEANT4 toolkit [23,29]). The tuned

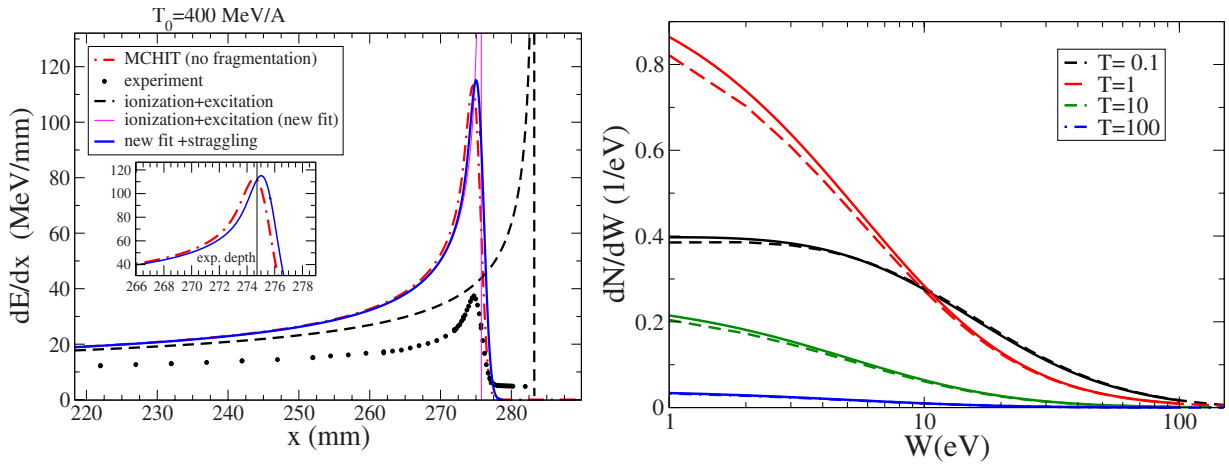


FIG. 1. (Color online) Linear energy deposition (left panel) for a carbon ion with incident energy of 400 MeV/u, computed with different parametrizations, within the experimental error of the original data, and compared to experiments [26] and MC simulations [23] (where no nuclear fragmentation is considered). The zoom in the inset shows also the experimental penetration depth. On the right panel the effect of this parametrization (solid line) on the spectra of secondary electrons compared to the previous one (dashed line).

TABLE IV. Bragg-peak positions for different incident energies of carbon ions in water obtained with the present parametrization with and without accounting for straggling and compared with experiments [25,26] and Monte Carlo simulations [23,29].

| $T$ (MeV/u) | Bragg-peak position (mm) | | | |
|---|---|---|---|---|
| | Us (single ion) | Us (straggling) | Schardt | MCHIT |
| 400 | 275.75 | 275.01 | 274.72 | 274.53 |
| 330 | 201.81 | 201.30 | 201.42 | 200.52 |
| 270 | 144.78 | 144.42 | 144.82 | 143.78 |
| 200 | 87.19 | 86.94 | 86.46 | 86.90 |
| 195 | 83.49 | 83.26 | 83.39 | |
| 135 | 44.20 | 44.05 | 43.34 | 43.73 |

parameters are shown in the third row of Table I. The same parametrization is applicable to a broad range of energies (see Table IV and Fig. 2), keeping the Bragg-peak position within the acceptable error for therapeutic uses (0.5 mm). In particular, the comparison with Monte Carlo simulations, shows on one hand an almost perfect agreement in the shape of the curves when considering only the electromagnetic processes and no nuclear fragmentation channels; as shown in the limit case of a 400 MeV/u ion beam (left panel of Fig. 1), where fragmentation has a drastic effect on the peak shape, but nevertheless does not affect the depth. On the other hand it reveals a slightly better reproducibility of the experimental depths in the whole range of energies for the present method (Table IV), as compared to MC, which is based on a single value of average excitation energy ($\langle I\rangle$=85 eV).

Thus, the approach suggested in Ref. [16] with the parameters given in Table I, can be used successfully also for rapid calculations of the Bragg-peak position; and, in case of limited nuclear fragmentations, as occur in smaller ions, may also provide a correct deposition profile depiction [30]. A similar procedure for energy spectra of electrons produced

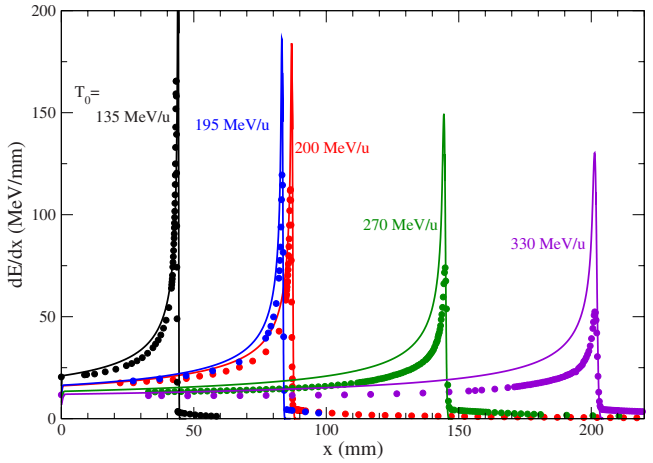


FIG. 2. (Color online) Linear energy deposition for carbon ions for different initial energies $T_0$: our model (all lines) compared to experiments from GSI [25,26] (all dots). Different labels (and colors) indicate curves at different initial ion-energies $T_0$.

by ions and by fast electrons has been performed by the Cucinotta group [19,20]. Our approach differs from the latter in the treatment of relativistic correction, the accounting for charge transfer, and in the parameter values for SDCSs.

## III. FAST REGIME

When ions are more energetic than 500 keV/u, the Born approximation is valid, and a direct connection with the experimental data for liquid water is possible through the dielectric-response model. This provides an opportunity for a more accurate calculation of the SDCS and thus the energy spectrum of secondary electrons.

### A. Dielectric-response model: Optical approximation

In this model, presented by a number of studies for electrons and protons [10,31], but rarely extended to heavier ions [13], the only parametric quantity is retrieved from measurements of photoionization cross sections. The main advantage of this model, which makes it suitable, especially for treating condensed media, is the simultaneous accounting for both single-particle and collective effects in the analysis of the response of a medium to the ionizing/exciting energetic particle. The key quantity is the energy-loss function, often denoted as $\eta_2$, derived by the dielectric function $\epsilon$ and directly connected to the generalized oscillator strength $df/dE(E,k)$ [32,33],

$$\eta_2(E,k) = \mathrm{Im}\left(\frac{-1}{\epsilon(E,k)}\right) = \frac{\pi\Omega_p^2}{2ZE}\frac{df(E,k)}{dE}, \tag{8}$$

where $Z$ is the total number of electrons of a molecule of the medium, $E$ is the transfered energy, $k$ is the transfered momentum, and $\Omega_p = 4R(\pi a_0^3 nZ)^{1/2} = 21.46$ eV is the plasma frequency computed for liquid water where $Z=10$.

Then, for a liquid medium, it is more convenient to insert a macroscopic cross section $\Lambda = n\sigma$, and consider [33]

$$\frac{d\Lambda}{dEdk} = \frac{z_{eff}^2 m_p}{\pi a_0 T}\frac{\eta_2(E,k)}{k}, \tag{9}$$

where the factor $m_p$ is the mass ratio between proton and electron, and, after integration over $k$,

$$\frac{d\Lambda}{dE} = \frac{z_{eff}^2 m_p}{\pi a_0 T}\int_{k_{\min}}^{k_{\max}} \eta_2(E,k)\frac{dk}{k}. \tag{10}$$

This can be expanded under the condition $E \ll T/m_p$ in the following sum:

$$\frac{d\Lambda}{dE} \simeq \frac{z_{eff}^2 m_p}{\pi a_0 T}\left[\frac{\eta_2(E,0)}{2}\ln\frac{T}{m_p R} + B(E) + O(Em_p/T)\right]. \tag{11}$$

In general, $\epsilon(E,k) = \epsilon_1(E,k) + i\epsilon_2(E,k)$, where both the real part $\epsilon_1$ and the imaginary part $\epsilon_2$ are derivable from experiments [34]. They are shown in Fig. 3 in the optical limit ($k=0$). Based on these functions, it is possible to derive $\eta_2$ vital for our calculations.

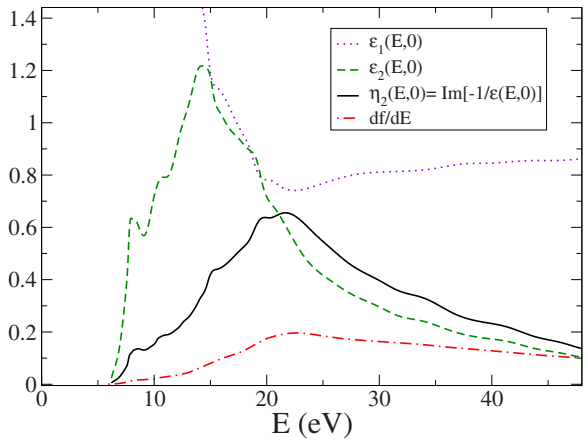


FIG. 3. (Color online) Dielectric function data retrievable by optical experimental data [34].

Thus, in cases where the optical limit is reasonable, i.e., when it is possible to consider ionization by ions to be similar to that of photons, it is possible to get a good approximation of the macroscopic cross section by retaining only the first term of Eq. (11), which is called Bethe optical term [11].

In passing from the energy loss to the secondary electron distribution, it is necessary to introduce the different ionization thresholds $I_j$ (here the real liquid-water data are used, second row of Table II) and contributions from different shells

$$\frac{d\Lambda}{dW} = \sum_j \frac{d\Lambda_j}{dW}$$

$$\frac{d\Lambda_j}{dW} \simeq \frac{z_{eff}^2 m_p}{\pi a_0 T}\left[\frac{G_j(E)\,\eta_2(W+I_j,0)}{2}\ln\frac{T}{m_p R} + B(E) + O(E/T)\right]. \tag{12}$$

The factors $G_j(E)$ account for different contributions to the optical spectrum from ionization of different shells. They are computed as suggested in a series of studies performed for protons Ref. [31] by treating separately the different transitions by decomposing the resulting optical data in a sum of Drude functions, with the constraints of respecting the sum rule,

$$\epsilon_2(E,0) = \sum_j^{ion} \epsilon_{2,ion}^{(j)}(E,0) + \sum_i^{exc} \epsilon_{2,exc}^{(i)}(E,0) \tag{13}$$

where the $\epsilon_{2,ion}^{(j)}$ and the $\epsilon_{2,exc}^{(i)}$ represent, respectively, the contributions of a given ionization or excitation mode to the total imaginary part of the dielectric function and are computed differently. In particular the ionization contributions are expressed well by conventional Drude functions,

$$\epsilon_{2,ion}^{(j)}(E,0) = \Omega_p^2 \frac{f_j \gamma_j E}{(E_j^2 - E^2) + (\gamma_j E)^2} \tag{14}$$

where the parameters $f_j, \gamma_j, E_j$ are respectively oscillator strength, width and position of the given transition and are found by imposing the sum rules,

TABLE V. Parameters (positions, widths and strengths) for the ionization transitions used for the shell contributions to $\epsilon_2$ [11].

| Shell | $E_j$ (eV) | $\gamma_j$ (eV) | $f_j$ |
|---|---|---|---|
| $1b_1$ | 16.30 | 14.00 | 0.2300 |
| $3a_1$ | 17.25 | 10.91 | 0.1600 |
| $1b_2$ | 28.00 | 27.38 | 0.1890 |
| $2a_1$ | 42.00 | 28.68 | 0.2095 |
| $1a_1$ | 450 | 360 | 0.3143 |

$$\int_0^\infty E\epsilon_2(E,0)dE = \Omega_p^2\pi/2 \tag{15}$$

$$\int_0^\infty E\eta_2(E,0)dE = \Omega_p^2\pi/2 \tag{16}$$

We use here the last fitted parameters from Ref. [11] (see Table V) for the single contributions, while we directly derived $\epsilon_1$ and $\epsilon_2$ from experiments in the region 1–50 eV, and extrapolating with a nonlinear curve fitting to the asymptotes (respectively, 1 and 0). Thus we take $G_j(E) = \epsilon_{2,ion}^{(j)}(E,0)/\epsilon_2(E,0)$. We can probe this approximation, as mentioned, under the condition of $E \ll T/m_p$; this turns out to be valid for relatively high $T(>0.5$ MeV), when considering the lower energy part of the secondary electron spectrum. From Fig. 4, we can see that compared to our parametric formalism, there is a region where the two approaches give very close results (10–40 eV), while at a lower energy the curve corresponding to the parametrization deviates, as it is not able to correctly reproduce the liquid medium, and at a higher electron energy the Bethe optical approximation is not valid; thus, the correct behavior is there described by the parametric, vaporlike curve.

### B. Dielectric-response model: Extension in the energy-momentum plane

Finer approaches extend to $k>0$, i.e., generating the full energy-momentum plane, characterized by the well-known

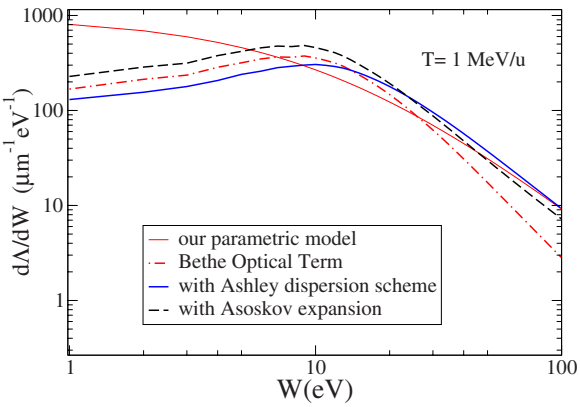


FIG. 4. (Color online) Energy spectra of secondary electrons induced by a carbon ion: Comparison between the parametric model and different dielectric-response model approaches for liquid water.

Bethe ridge [35], through different models, usually called dispersion schemes. These models follow the requirements to generate a generalized energy-loss function $\eta_2(E,k)$ obviously consistent in the optical limit $(k\to 0)$ to the corresponding optical function, as well as in the asymptotic behavior for large momentum transfer to the free-electron limit,

$$\lim_{k\to\infty} \eta_2(E,k) \sim \delta(E-Q), \tag{17}$$

where $Q=k^2/2m$ is the free-electron recoil energy [36]. Many methods have been proposed, such as the one by Ashley [37], based on a $\delta$-function representation of the optical oscillator strength of an atom

$$\frac{df(E)}{dE} = \sum_j f_j \delta(E-E_j) \tag{18}$$

(with $f_j$ and $E_j$ respectively height and position of a given energy transition), where $E_j$ is extended for $k>0$ to $E_j+Q$ and a generalization to condensed matter is performed:

$$\eta_2(E,k) = \int_0^\infty \frac{E'}{E}\eta_2(E',0)\delta[E-(E'+Q)]dE'$$
$$= \frac{E-Q}{E}\eta_2(E-Q,0)\Theta(E-Q) \tag{19}$$

where $\Theta(E-Q)$ is a step function, equal to 1 for $E>Q$ and 0 otherwise. The $k$ dependence from the optical data is then achieved.

Assuming that the weights computed in the case of 0 momentum transfer do not change significantly, it is then possible to assume $G(E,k)=G(E)$ and compute the contributions to ionization of the shells with the Eq. (19) and

$$\frac{d\Lambda_j(E,k)}{dW} = \frac{z_{eff}^2 m_p}{\pi a_0 T}\int_{k_{\min}}^{k_{\max}} G_j(E)\eta_2(E,k)\frac{dk}{k}. \tag{20}$$

The integration in $k$, as shown in Eq. (10), is then performed with the minimum and maximum momentum transfer as the integration limits,

$$k_\pm = \sqrt{2m}(\sqrt{T} \pm \sqrt{T-E}). \tag{21}$$

Thorough reviews of the various possibility to expand in the Bethe surface are available in Refs. [38,39]. Other approaches include also a way for accounting the relativistic regime of the projectile energy. In general, this correction is small in the energy ranges where the main focus of the interest in the evaluation of electrons spectra is (Bragg-peak region, i.e., $T<10$ MeV/u, where $\beta^2<10^{-2}$). We report here, anyway, the results obtained by using such an approach, suggested by Asoskov *et al.* [40], extended by us from an atomic single shell system to include a multishell target. This formalism uses a different method but performs still a similar expansion in the energy-momentum plane by accounting for the recoil energy in order to express the generalized oscillator strength (GOS) as a function of the optical oscillator strength (OOS). That, after integration in $k$, brings to the formula:

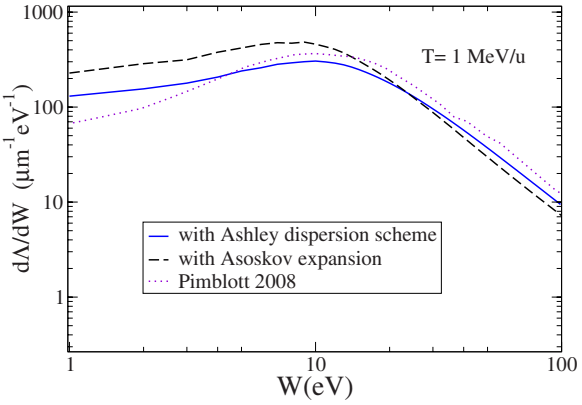


FIG. 5. (Color online) Energy spectra of secondary electrons induced by a carbon ion: Comparison between the reported models and Ref. [13].

$$\frac{d\Lambda}{dW} = \sum_j \frac{d\Lambda_j}{dW},$$

$$\frac{d\Lambda_j}{dW} = \frac{8a_0^2R^2N_i z_{eff}Z}{\Omega_p^2 mV^2}\left[\frac{E\epsilon_{2,ion}^{(j)}(E)}{E\epsilon^2}\left(\ln\frac{2mV^2}{E|1-\beta^2\epsilon|}\right.\right.$$
$$\left.\left. - \frac{\epsilon_1-\beta^2\epsilon^2}{\epsilon_2}\arctan\frac{-\beta^2\epsilon_2}{1-\beta^2\epsilon_1}\right) + \frac{F(E)}{E^2}\right] \tag{22}$$

where

$$F(E) = \int_0^E \frac{E'\epsilon_{2,ion}^{(j)}(E')}{\epsilon^2}dE' \tag{23}$$

and, for each shell, $E=W+I_i$.

In Fig. 4, one can appreciate corrections induced by these approaches to the Bethe optical term, which is reliable only for very small values of $W$, as expected. We can see how the parametric and other curves are almost coincident at large $W$, where the medium differences are less dramatic. Finally, in Fig. 5 we report a comparison with another model [13]. Reference [13] uses a stochastic simulation for the partition of the different shells, and reports only normalized values (hereby scaled for the present total cross section); these results are smaller compared to ours at very low electron energies, while they are very close to ours for the energies above 3 eV. This lower region of course is still very important, thus a further improvement of detail of the energy shape, with the help of further experiments, is desirable.

## IV. CONCLUSIONS

This paper gives an opportunity to calculate the energy spectra of secondary electrons produced by energetic ions incident on tissue, mimicked by liquid water. In order to report these electron energy distributions with the best possible accuracy for each ion energy range, we consider different approaches.

The energy distributions of secondary electrons produced by low-energy ions are obtained using a general parametrization based on the Rudd Model with parameters modified

for liquid water distinguished from the original parameters fitted to experiments with water vapor. The present parameters were obtained by fitting the depths of Bragg peaks (for different incident energies) to the experiments done at GSI. The obtained parametrization can be used for a fast calculation of the position of the Bragg peak for a given energy of the projectile with a therapeutically accepted precision. An advantage of such parametrization is its universality for different applications and its analyticity, which makes all calculations fast.

For higher ion energies, the dielectric-response approach, previously tested for protons, and herein applied for heavier ions, is shown to be successful in describing the details of secondary electron spectra profiles. We compare two approaches and show that they can be used for different values of secondary electron energies.

The results of this work can be used for calculations of realistic radial dose distributions at different depths along the ion's trajectory. Such calculations, if rapid enough, are important for calculating the relative biological effectiveness and treatment planning.

Further experiments, combining more realistic projectiles (heavier ions, since the direct ionization data are only available for protons and helium ions [17]) and more realistic media, are very much desired.

## ACKNOWLEDGMENTS

This work is partially supported by the European Commission within the Network of Excellence project EXCELL, the Deutsche Forschungsgemeinschaft and a FIAS fellowship. We are grateful to D. Schardt and I. Pshenichnov for providing original experimental and Monte Carlo data, and to A. V. Korol and I. Mishustin for multiple fruitful discussions. J. S. Payson's help is greatly appreciated.

[1] U. Amaldi and G. Kraft, Rep. Prog. Phys. **68**, 1861 (2005).
[2] F. A. Cucinotta and M. Durante, Lancet Oncol. **7**, 431 (2006).
[3] A. V. Solov'yov, E. Surdutovich, E. Scifoni, I. Mishustin, and W. Greiner, Phys. Rev. E **79**, 011909 (2009).
[4] E. Surdutovich and A. V. Solov'yov, Europhys. News **40** (2), 21 (2009).
[5] M. Toulemonde, E. Surdutovich, and A. V. Solovyov, Phys. Rev. E **80**, 031913 (2009).
[6] D. T. Goodhead, Radiat. Prot. Dosim. **122**, 3 (2006).
[7] H. Nikjoo, P. O'Neill, M. Terrisol, and D. T. Goodhead, Radiat. Environ. Biophys. **38**, 31 (1999).
[8] H. Nikjoo, S. Uehara, D. Emfietzoglou, and F. A. Cucinotta, Radiat. Meas. **41**, 1052 (2006).
[9] B. Boudaiffa, P. Cloutier, D. Hunting, M. A. Huels, and L. Sanche, Science **287**, 1658 (2000).
[10] M. Dingfelder, M. Inokuti, and H. G. Paretzke, Radiat. Phys. Chem. **59**, 255 (2000).
[11] D. Emfietzoglou and H. Nikjoo, Radiat. Res. **163**, 98 (2005).
[12] S. Uehara and H. Nikjoo, J. Phys. Chem. B **106**, 11051 (2002).
[13] S. M. Pimblott and J. A. LaVerne, Rad. Phys. Chem. **76**, 1244 (2007).
[14] H. Tsujii *et al.*, New J. Phys. **10**, 075009 (2008).
[15] O. I. Obolensky, E. Surdutovich, I. Pshenichnov, I. Mishustin, A. V. Solov'yov, and W. Greiner, Nucl. Instrum. Methods Phys. Res. B **266**, 1623 (2008).
[16] E. Surdutovich, O. I. Obolensky, E. Scifoni, I. Pshenichnov, I. Mishustin, A. V. Solov'yov, and W. Greiner, Eur. Phys. J. D **51**, 63 (2009).
[17] L. H. Toburen, W. E. Wilson, and R. J. Popowich, Radiat. Res. **82**, 27 (1980).
[18] M. E. Rudd, Y.-K. Kim, D. H. Madison, and T. Gay, Rev. Mod. Phys. **64**, 441 (1992).
[19] I. Plante and F. A. Cucinotta, New J. Phys. **11**, 063047 (2009).
[20] I. Plante and F. A. Cucinotta, New J. Phys. **10**, 125020 (2008).
[21] W. H. Barkas, *Nuclear Research Emulsions I. Techniques and Theory* (Academic Press Inc., New York, London, 1963), Vol. 1, p. 371.
[22] E. Scifoni, E. Surdutovich, A. V. Solov'yov, I. Pshenichnov, I. Mishustin, and W. Greiner, in *Proceedings of the 5th International Conference (RADAM 2008)*, edited by K. Tokesi and B. Sulik, AIP Conf. Proc. No. 1080, (AIP, Melville, New York, 2008) p. 104.
[23] I. Pshenichnov, I. Mishustin, and W. Greiner, Nucl. Instrum. Methods Phys. Res. B **266**, 1094 (2008).
[24] ICRU Report No. 49, 1993.
[25] L. Sihver *et al.*, Jpn. J. Med. Phys. **18**, 1 (1998).
[26] E. Haettner, H. Iwase, and D. Schardt, Radiat. Prot. Dosim. **122**, 485 (2006).
[27] J. H. Miller and A. E. S. Green, Radiat. Res. **54**, 343 (1973).
[28] W. T. Chu, B. A. Ludewigt, and T. R. Renner, Rev. Sci. Instrum. **64**, 2055 (1993).
[29] I. Pshenichnov (private communication).
[30] E. Scifoni, E. Surdutovich, and A. V. Solov'yov, in *The Fourth International Symposium on Atomic Cluster Collisions (ISACC 2009)*, edited by A. V. Solov'yov and E. Surdutovich, AIP Conf. Proc. No. 1197 (AIP, Melville, New York, 2009) p, 217.
[31] D. Emfietzoglou and M. Moscovitch, Nucl. Instrum. Methods Phys. Res. B **209**, 239 (2003).
[32] L. D. Landau and E. M. Lifshitz, *Electrodynamics of Continuous Media* (Pergamon Press, London, 1970).
[33] M. Inokuti, Rev. Mod. Phys. **43**, 297 (1971).
[34] H. Hayashi, N. Watanabe, Y. Udagawa, and C.-C. Kao, Proc. Natl. Acad. Sci. U.S.A. **97**, 6264 (2000).
[35] M. Dingfelder, D. Hantke, M. Inokuti, and H. G. Paretzke, Radiat. Phys. Chem. **53**, 1 (1998).
[36] J. M. Fernandez-Varea *et al.*, J. Phys.: Condens. Matter **5**, 3593 (1993).
[37] J. C. Ashley, J. Electron Spectrosc. Relat. Phenom. **46**, 199 (1988).
[38] D. Emfietzoglou, F. A. Cucinotta, and H. Nikjoo, Radiat. Res. **164**, 202 (2005).
[39] M. Dingfelder R. H. Ritchie J. E. Turner, W. Friedland, H. G. Paretzke, and R. N. Hamm, Radiat. Res. **169**, 584 (2008).
[40] V. S. Asoskov, V. M. Grichin, V. K. Ermilova, L. P. Kotenko, G. I. Merson, and V. A. Chechin, Lebedev Phys. Inst. Bull. **140**, 3 (1982).